Available online at www.sciencedirect.com
SCIENCE DIRECT®
Journal of Sound and Vibration 290 (2006) 690–704
JOURNAL OF SOUND AND VIBRATION
www.elsevier.com/locate/jsvi

Three-dimensional free vibration analysis of plates using the *h-p* version of the finite element method

A. Houmat*

Department of Mechanical Engineering, Faculty of Engineering, University of Tlemcen, Tlemcen 13000, Algeria

Received 30 March 2004; received in revised form 11 November 2004; accepted 19 April 2005
Available online 8 August 2005

Abstract

The *h-p* version of the finite element method based on a pentahedral *p*-element is applied to three-dimensional free vibrations of plates. The element's new hierarchical shape functions are expressed in terms of the shifted Legendre orthogonal polynomials. The accuracy of the solution can be improved by simultaneously refining the mesh and increasing the polynomial order. The method is capable of providing a full frequency spectrum including both the in-plane and the out-of-plane modes. Results of frequency calculations are first found for a skew plate on a soft edge support and a cantilevered right isosceles triangular plate and comparisons are made with other methods. Results are also found for a square plate on a hard edge support and comparisons are made with two-dimensional plate theories. Furthermore, highly accurate values for a free hexagonal plate are presented for the first time.

1. Introduction

Two-dimensional plate theories reduce the dimensionality of the problem from three to two by making certain assumptions on the stresses in the direction normal to the plate middle surface. These assumptions greatly simplify the analysis and reduce the computational effort but also introduce errors. Since a free vibration analysis based on three-dimensional elasticity theory makes no simplifying assumptions it provides realistic results and brings out physical insights which cannot be predicted by the two-dimensional theories. Up to date, the research on three-dimensional free vibration analysis has

*Tel./fax: +213 43 20 15 34.
E-mail address: a_houmat@wissal.dz.

0022-460X/$ - see front matter © 2005 Elsevier Ltd. All rights reserved.
doi:10.1016/j.jsv.2005.04.024

Nomenclature

x, y, z	rectangular Cartesian coordinates
ξ_1, ξ_2, ξ_3	non-dimensional area coordinates
$\zeta = 2z/h$	non-dimensional coordinate
A	surface area of element triangular faces
u, v, w	displacements in x, y, z directions
p	polynomial order
ρ	mass density
E	modulus of elasticity
$G = E/2(1+v)$	shear modulus of elasticity
v	Poisson's ratio
h	plate thickness
$\mathbf{k}_{\alpha,\beta}$	element stiffness matrix
$\mathbf{m}_{\alpha,\beta}$	element mass matrix
$\mathbf{q}_\beta$	element vector of generalized displacements
M	order of element stiffness and mass matrices
$\mathbf{K}$	global stiffness matrix
$\mathbf{M}$	global mass matrix
$\mathbf{Q}$	global vector of generalized displacements
t	time
ω	natural frequency
$\Omega = \omega\sqrt{\rho/G}$	frequency parameter

been limited to developing accurate methods which are mainly suitable for plates of simple geometry (rectangular, skew, triangular). The most recent of these works are attributed to Liew et al. [1], Cheung and Zhou [2], and Zhou et al. [3]. Thus, the development of an accurate more general three-dimensional free vibration analysis is necessary to deal with plates of complex geometry. The highly accurate *h-p* version of the finite element method is able to fulfill this goal.

The *h-p* version of the finite element method has been applied to a two-dimensional problem of a vibrating membrane [4] and has been shown to offer considerable savings in computational effort when compared with the standard *h*-version of the finite element method. The present work implements for the first time the *h-p* version of the finite element method based on a pentahedral *p*-element to three-dimensional free vibrations of plates. The method can provide a full frequency spectrum including both the in-plane and the out-of-plane modes.

The hierarchical shape functions for a pentahedral *p*-element combine the shape functions for a triangular *p*-element and those for a one-dimensional *p*-element. These shape functions were expressed by Szabo and Babuska [5] in terms of the Legendre orthogonal polynomials. In this paper, new simple expressions of the hierarchical shape functions for the pentahedral *p*-element are given in terms of the shifted Legendre orthogonal polynomials which are more suitable for this type of element because they are defined in the same interval as area coordinates.

A skew plate on a soft edge support and a cantilevered isosceles triangular plate are first considered to assess the convergence and accuracy of the present method. A square plate on a hard edge support is also considered to assess the accuracy of two-dimensional plate theories. Furthermore, a free hexagonal plate is analyzed to show the applicability of the present method to plates of more complex domains.

2. Formulation

2.1. The shape functions

A pentahedral element is shown in Fig. 1. The dimensionless coordinates ξ_2, ξ_3 and ζ are also shown in the figure. A dependent dimensionless coordinate ξ_1 $(= 1 - \xi_2 - \xi_3)$ is introduced.

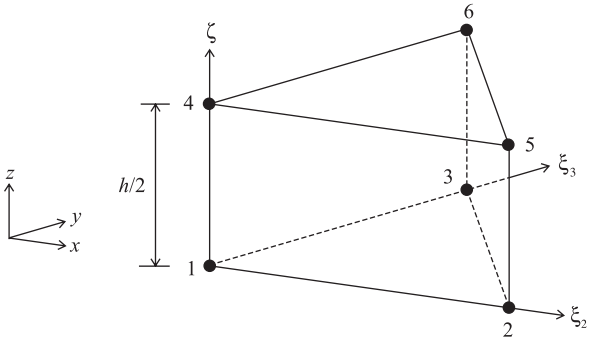

Fig. 1. The pentahedral element coordinates.

The shape functions for a pentahedral p-element $g_\beta(\xi_1, \xi_2, \xi_3, \zeta)$ ($\beta = 1,2,3,...,N$) consist of:

- Six nodal shape functions:

$$\xi_1(1-\zeta), \quad \xi_2(1-\zeta), \quad \xi_3(1-\zeta), \quad \xi_1\zeta, \quad \xi_2\zeta, \quad \xi_3\zeta \tag{1}$$

- $(p-1)$ shape functions on edge 1-2:

$$\xi_1\xi_2 P_i^*(\xi_2)(1-\zeta), \tag{2}$$

- $(p-1)$ shape functions on edge 2-3:

$$\xi_2\xi_3 P_j^*(\xi_3)(1-\zeta), \tag{3}$$

- $(p-1)$ shape functions on edge 1-3:

$$\xi_1\xi_3 P_j^*(\xi_3)(1-\zeta), \tag{4}$$

- $(p-1)$ shape functions on edge 4-5:

$$\xi_1\xi_2 P_i^*(\xi_2)\zeta, \tag{5}$$

- $(p-1)$ shape functions on edge 5-6:

$$\xi_2\xi_3 P_j^*(\xi_3)\zeta, \tag{6}$$

- $(p-1)$ shape functions on edge 4-6:

$$\xi_1\xi_3 P_j^*(\xi_3)\zeta, \tag{7}$$

- $(p-1)$ shape functions on edge 1-4:

$$\xi_1\phi_{k+2}(\zeta), \tag{8}$$

- $(p-1)$ shape functions on edge 2-5:

$$\xi_2\phi_{k+2}(\zeta), \tag{9}$$

- $(p-1)$ shape functions on edge 3-6:

$$\xi_3\phi_{k+2}(\zeta), \tag{10}$$

where $i,j,k=0,1,2,\ldots,p-2$.

- $(p-1)(p-2)/2$ shape functions on face 1-2-3:

$$\xi_1\xi_2\xi_3P_i^*(\xi_2)P_j^*(\xi_3)(1-\zeta), \tag{11}$$

- $(p-1)(p-2)/2$ shape functions on face 4-5-6:

$$\xi_1\xi_2\xi_3P_i^*(\xi_2)P_j^*(\xi_3)\zeta, \tag{12}$$

where $i,j=0,1,2,\ldots,p-3$ and $i+j=0,1,2,\ldots,p-3$.

- $(p-2)(p-3)/2$ shape functions on face 1-2-5-4:

$$\xi_1\xi_2P_i^*(\xi_2)\phi_{k+2}(\zeta), \tag{13}$$

- $(p-2)(p-3)/2$ shape functions on face 3-2-5-6:

$$\xi_2\xi_3P_j^*(\xi_3)\phi_{k+2}(\zeta), \tag{14}$$

- $(p-2)(p-3)/2$ shape functions on face 1-3-6-4:

$$\xi_1\xi_3P_j^*(\xi_3)\phi_{k+2}(\zeta), \tag{15}$$

where $j,k=0,1,2,\ldots,p-4$ and $j+k=0,1,2,\ldots,p-4$.

- $(p-2)(p-3)(p-4)/6$ shape functions in the interior of the element:

$$\xi_1\xi_2\xi_3P_i^*(\xi_2)P_j^*(\xi_3)\phi_{k+2}(\zeta), \tag{16}$$

where $i,j,k=0,1,2,\ldots,p-5$ and $i+j+k=0,1,2,\ldots,p-5$.

In the above, P_r^* denotes the rth order shifted Legendre orthogonal polynomial and ϕ_r is a function which is defined as

$$\phi_r(\zeta)=\frac{1}{2(2r-1)}[P_r^*(\zeta)-P_{r-2}^*(\zeta)]. \tag{17}$$

The hierarchical shape functions $g_\beta(\xi_1,\xi_2,\xi_3,\zeta)$ $(\beta=1,2,3,...,64)$ for $p\leqslant 5$ are shown in Table 1. They are ordered in a way to preserve the hierarchical property of the element.

Table 1
The hierarchical shape functions for a pentahedral p-element ($p \leqslant 5$)

β	g_β	β	g_β
1	$\xi_1(1-\zeta)$	33	$\xi_1(5\zeta^4-10\zeta^3+6\zeta^2-\zeta)$
2	$\xi_2(1-\zeta)$	34	$\xi_2(5\zeta^4-10\zeta^3+6\zeta^2-\zeta)$
3	$\xi_3(1-\zeta)$	35	$\xi_3(5\zeta^4-10\zeta^3+6\zeta^2-\zeta)$
4	$\xi_1\zeta$	36	$\xi_1\xi_2\xi_3(2\xi_2-1)(1-\zeta)$
5	$\xi_2\zeta$	37	$\xi_1\xi_2\xi_3(2\xi_3-1)(1-\zeta)$
6	$\xi_3\zeta$	38	$\xi_1\xi_2\xi_3(2\xi_2-1)\zeta$
7	$\xi_1\xi_2(1-\zeta)$	39	$\xi_1\xi_2\xi_3(2\xi_3-1)\zeta$
8	$\xi_2\xi_3(1-\zeta)$	40	$\xi_1\xi_2(\zeta^2-\zeta)$
9	$\xi_1\xi_3(1-\zeta)$	41	$\xi_2\xi_3(\zeta^2-\zeta)$
10	$\xi_1\xi_2\zeta$	42	$\xi_1\xi_3(\zeta^2-\zeta)$
11	$\xi_2\xi_3\zeta$	43	$\xi_1\xi_2(20\xi_2^3-30\xi_2^2+12\xi_2-1)(1-\zeta)$
12	$\xi_1\xi_3\zeta$	44	$\xi_2\xi_3(20\xi_3^3-30\xi_3^2+12\xi_3-1)(1-\zeta)$
13	$\xi_1(\zeta^2-\zeta)$	45	$\xi_1\xi_3(20\xi_3^3-30\xi_3^2+12\xi_3-1)(1-\zeta)$
14	$\xi_2(\zeta^2-\zeta)$	46	$\xi_1\xi_2(20\xi_2^3-30\xi_2^2+12\xi_2-1)\zeta$
15	$\xi_3(\zeta^2-\zeta)$	47	$\xi_2\xi_3(20\xi_3^3-30\xi_3^2+12\xi_3-1)\zeta$
16	$\xi_1\xi_2(2\xi_2-1)(1-\zeta)$	48	$\xi_1\xi_3(20\xi_3^3-30\xi_3^2+12\xi_3-1)\zeta$
17	$\xi_2\xi_3(2\xi_3-1)(1-\zeta)$	49	$\xi_1(14\zeta^5-35\zeta^4+30\zeta^3-10\zeta^2+\zeta)$
18	$\xi_1\xi_3(2\xi_3-1)(1-\zeta)$	50	$\xi_2(14\zeta^5-35\zeta^4+30\zeta^3-10\zeta^2+\zeta)$
19	$\xi_1\xi_2(2\xi_2-1)\zeta$	51	$\xi_3(14\zeta^5-35\zeta^4+30\zeta^3-10\zeta^2+\zeta)$
20	$\xi_2\xi_3(2\xi_3-1)\zeta$	52	$\xi_1\xi_2\xi_3(6\xi_2^2-6\xi_2+1)(1-\zeta)$
21	$\xi_1\xi_3(2\xi_3-1)\zeta$	53	$\xi_1\xi_2\xi_3(6\xi_3^2-6\xi_3+1)(1-\zeta)$
22	$\xi_1(2\zeta^3-3\zeta^2+\zeta)$	54	$\xi_1\xi_2\xi_3(2\xi_2-1)(2\xi_3-1)(1-\zeta)$
23	$\xi_2(2\zeta^3-3\zeta^2+\zeta)$	55	$\xi_1\xi_2\xi_3(6\xi_2^2-6\xi_2+1)\zeta$
24	$\xi_3(2\zeta^3-3\zeta^2+\zeta)$	56	$\xi_1\xi_2\xi_3(6\xi_3^2-6\xi_3+1)\zeta$
25	$\xi_1\xi_2\xi_3(1-\zeta)$	57	$\xi_1\xi_2\xi_3(2\xi_2-1)(2\xi_3-1)\zeta$
26	$\xi_1\xi_2\xi_3\zeta$	58	$\xi_1\xi_2(2\zeta^3-3\zeta^2+\zeta)$
27	$\xi_1\xi_2(6\xi_2^2-6\xi_2+1)(1-\zeta)$	59	$\xi_1\xi_2(2\xi_2-1)(\zeta^2-\zeta)$
28	$\xi_2\xi_3(6\xi_3^2-6\xi_3+1)(1-\zeta)$	60	$\xi_2\xi_3(2\zeta^3-3\zeta^2+\zeta)$
29	$\xi_1\xi_3(6\xi_3^2-6\xi_3+1)(1-\zeta)$	61	$\xi_2\xi_3(2\xi_3-1)(\zeta^2-\zeta)$
30	$\xi_1\xi_2(6\xi_2^2-6\xi_2+1)\zeta$	62	$\xi_1\xi_3(2\zeta^3-3\zeta^2+\zeta)$
31	$\xi_2\xi_3(6\xi_3^2-6\xi_3+1)\zeta$	63	$\xi_1\xi_3(2\xi_3-1)(\zeta^2-\zeta)$
32	$\xi_1\xi_3(6\xi_3^2-6\xi_3+1)\zeta$	64	$\xi_1\xi_2\xi_3(\zeta^2-\zeta)$

2.2. The p-element stiffness and mass matrices

The potential energy U and kinetic energy T of the pentahedral p-element are

$$U=\frac{E}{2(1+\nu)(1-2\nu)}\int_0^{h/2}\int_A\left\{(1-\nu)\left[\left(\frac{\partial u}{\partial x}\right)^2+\left(\frac{\partial v}{\partial y}\right)^2+\left(\frac{\partial w}{\partial z}\right)^2\right]\right.$$

$$+2\nu\left[\left(\frac{\partial u}{\partial x}\right)\left(\frac{\partial v}{\partial y}\right)+\left(\frac{\partial u}{\partial x}\right)\left(\frac{\partial w}{\partial z}\right)+\left(\frac{\partial v}{\partial y}\right)\left(\frac{\partial w}{\partial z}\right)\right]$$
$$+\frac{(1-2\nu)}{2}\left[\left(\frac{\partial u}{\partial y}+\frac{\partial v}{\partial x}\right)^2+\left(\frac{\partial u}{\partial z}+\frac{\partial w}{\partial x}\right)^2+\left(\frac{\partial v}{\partial z}+\frac{\partial w}{\partial y}\right)^2\right]\Bigg\}\,\mathrm{d}A\,\mathrm{d}z, \tag{18}$$

$$T=\frac{\rho}{2}\int_0^{h/2}\int_A(\dot{u}^2+\dot{v}^2+\dot{w}^2)\,\mathrm{d}A\,\mathrm{d}z, \tag{19}$$

where the dot denotes differentiation with respect to time.

The above equations may be expressed in terms of the dimensionless coordinates as

$$U=\frac{EhA}{2(1+\nu)(1-2\nu)}\int_0^1\int_0^1\int_0^{1-\xi_3}\Bigg\{(1-\nu)\left[\left(\sum_{n=1}^3\frac{a_n}{2A}\frac{\partial u}{\partial\xi_n}\right)^2+\left(\sum_{n=1}^3\frac{b_n}{2A}\frac{\partial v}{\partial\xi_n}\right)^2+\left(\frac{2}{h}\frac{\partial w}{\partial\zeta}\right)^2\right]$$
$$+2\nu\left[\left(\sum_{n=1}^3\frac{a_n}{2A}\frac{\partial u}{\partial\xi_n}\right)\left(\sum_{n=1}^3\frac{b_n}{2A}\frac{\partial v}{\partial\xi_n}\right)+\left(\sum_{n=1}^3\frac{a_n}{2A}\frac{\partial u}{\partial\xi_n}\right)\left(\frac{2}{h}\frac{\partial w}{\partial\zeta}\right)+\left(\sum_{n=1}^3\frac{b_n}{2A}\frac{\partial v}{\partial\xi_n}\right)\left(\frac{2}{h}\frac{\partial w}{\partial\zeta}\right)\right]$$
$$+\frac{(1-2\nu)}{2}\left[\left(\sum_{n=1}^3\frac{b_n}{2A}\frac{\partial u}{\partial\xi_n}+\sum_{n=1}^3\frac{a_n}{2A}\frac{\partial v}{\partial\xi_n}\right)^2+\left(\frac{2}{h}\frac{\partial u}{\partial\zeta}+\sum_{n=1}^3\frac{a_n}{2A}\frac{\partial w}{\partial\xi_n}\right)^2\right.$$
$$\left.+\left(\frac{2}{h}\frac{\partial v}{\partial\zeta}+\sum_{n=1}^3\frac{b_n}{2A}\frac{\partial w}{\partial\xi_n}\right)^2\right]\Bigg\}\,\mathrm{d}\xi_2\,\mathrm{d}\xi_3\,\mathrm{d}\zeta, \tag{20}$$

$$T=\frac{\rho hA}{2}\int_0^1\int_0^1\int_0^{1-\xi_3}(\dot{u}^2+\dot{v}^2+\dot{w}^2)\,\mathrm{d}\xi_2\,\mathrm{d}\xi_3\,\mathrm{d}\zeta, \tag{21}$$

where the parameters a_n and b_n are defined in terms of the nodal x and y coordinates as

$$a_1=x_3-x_2=x_6-x_5,\quad a_2=x_1-x_3=x_4-x_6,\quad a_3=x_2-x_1=x_5-x_4, \tag{22}$$

$$b_1=y_2-y_3=y_5-y_6,\quad b_2=y_3-y_1=y_6-y_4,\quad b_3=y_1-y_2=y_4-y_5. \tag{23}$$

The displacement vector in this element may expressed as

$$\begin{Bmatrix}u\\v\\w\end{Bmatrix}=\sum_{\beta=1}^{N}\mathbf{N}_\beta\mathbf{q}_\beta, \tag{24}$$

where

$$\mathbf{N}_\beta=\begin{bmatrix}g_\beta(\xi_1,\xi_2,\xi_3,\zeta) & 0 & 0\\ 0 & g_\beta(\xi_1,\xi_2,\xi_3,\zeta) & 0\\ 0 & 0 & g_\beta(\xi_1,\xi_2,\xi_3,\zeta)\end{bmatrix} \tag{25}$$

and

$$\mathbf{q}_\beta = \begin{Bmatrix} q_{3\beta-2}(t) \\ q_{3\beta-1}(t) \\ q_{3\beta}(t) \end{Bmatrix}. \tag{26}$$

Substituting Eq. (24) into Eqs. (20) and (21) gives

$$U = \frac{1}{2}\sum_{\alpha=1}^{N}\sum_{\beta=1}^{N} \mathbf{q}_\alpha^{\mathrm{T}} \mathbf{k}_{\alpha,\beta} \mathbf{q}_\beta, \tag{27}$$

$$T = \frac{1}{2}\sum_{\alpha=1}^{N}\sum_{\beta=1}^{N} \dot{\mathbf{q}}_\alpha^{\mathrm{T}} \mathbf{m}_{\alpha,\beta} \dot{\mathbf{q}}_\beta, \tag{28}$$

where

$$\mathbf{k}_{\alpha,\beta} = \begin{bmatrix} k_{3\alpha-2,3\beta-2} & k_{3\alpha-2,3\beta-1} & k_{3\alpha-2,3\beta} \\ k_{3\alpha-1,3\beta-2} & k_{3\alpha-1,3\beta-1} & k_{3\alpha-1,3\beta} \\ k_{3\alpha,3\beta-2} & k_{3\alpha,3\beta-1} & k_{3\alpha,3\beta} \end{bmatrix} \tag{29}$$

and

$$\mathbf{m}_{\alpha,\beta} = \begin{bmatrix} m_{3\alpha-2,3\beta-2} & m_{3\alpha-2,3\beta-1} & m_{3\alpha-2,3\beta} \\ m_{3\alpha-1,3\beta-2} & m_{3\alpha-1,3\beta-1} & m_{3\alpha-1,3\beta} \\ m_{3\alpha,3\beta-2} & m_{3\alpha,3\beta-1} & m_{3\alpha,3\beta} \end{bmatrix}. \tag{30}$$

The coefficients of the pentahedral p-element stiffness and mass matrices are given in Appendix A. They are expressed in terms of the following integrals:

$$A_{\alpha,\beta}^{m,n} = \int_0^1 \int_0^1 \int_0^{1-\xi_3} \frac{\mathrm{d}g_\alpha}{\mathrm{d}\xi_m}\frac{\mathrm{d}g_\beta}{\mathrm{d}\xi_n}\,\mathrm{d}\xi_2\,\mathrm{d}\xi_3\,\mathrm{d}\zeta, \tag{31}$$

$$B_{\alpha,\beta}^{m} = \int_0^1 \int_0^1 \int_0^{1-\xi_3} \frac{\mathrm{d}g_\alpha}{\mathrm{d}\xi_m}\frac{\mathrm{d}g_\beta}{\mathrm{d}\zeta}\,\mathrm{d}\xi_2\,\mathrm{d}\xi_3\,\mathrm{d}\zeta, \tag{32}$$

$$C_{\alpha,\beta}^{n} = \int_0^1 \int_0^1 \int_0^{1-\xi_3} \frac{\mathrm{d}g_\alpha}{\mathrm{d}\zeta}\frac{\mathrm{d}g_\beta}{\mathrm{d}\xi_n}\,\mathrm{d}\xi_2\,\mathrm{d}\xi_3\,\mathrm{d}\zeta, \tag{33}$$

$$D_{\alpha,\beta} = \int_0^1 \int_0^1 \int_0^{1-\xi_3} \frac{\mathrm{d}g_\alpha}{\mathrm{d}\zeta}\frac{\mathrm{d}g_\beta}{\mathrm{d}\zeta}\,\mathrm{d}\xi_2\,\mathrm{d}\xi_3\,\mathrm{d}\zeta, \tag{34}$$

$$E_{\alpha,\beta} = \int_0^1 \int_0^1 \int_0^{1-\xi_3} g_\alpha g_\beta\,\mathrm{d}\xi_2\,\mathrm{d}\xi_3\,\mathrm{d}\zeta. \tag{35}$$

The above integrals can be calculated exactly by first substituting $1-\xi_2-\xi_3$ for ξ_1 in the integrand and then by using symbolic computing.

The order of the element stiffness and mass matrices is

$$M = 3N = \tfrac{1}{2}(p+3)(p^2+3p+8). \tag{36}$$

The integrals required to evaluate the element stiffness and mass matrices up to a maximal value of p equal to 8 were calculated exactly using symbolic computing.

The processes of assembly of p-elements and application of boundary conditions are discussed in Ref. [4].

Assuming harmonic motion, the governing equations of free motion can be obtained by substituting the resultant global stiffness and mass matrices into Lagrange's equations. This leads to the following equations:

$$[\mathbf{K} - \omega^2\mathbf{M}]\mathbf{Q} = \mathbf{0}. \tag{37}$$

The above generalized eigenvalue problem can be solved using any known technique to yield the natural frequencies.

3. Results

It is well-known that the frequencies obtained by the h-p version of the finite element method converge from above to the exact values. Thus, these values are upper-bounds to the exact ones. These upper-bounds can be improved by simultaneously refining the mesh and increasing the polynomial order.

In all the applications described in this section, the value of Poisson's ratio is taken to be 0.3. The results of frequency calculation are presented in tabular format. In the tables, NEL and NDOF denote, respectively, the number of elements and the number of degrees of freedom used in the h-p version of the finite element method.

Two examples were first considered to assess the convergence and accuracy of the h-p version of the finite element method. The two examples were chosen because solutions were available for comparison. The first example is a moderately thick skew plate with a soft simple support condition and $h = 0.2$ (Fig. 2). Such a support condition means that the supported edge is only restrained in the transverse direction (i.e. the out-of-plane displacement is zero). The soft support condition is so called to distinguish it from the hard support condition which means a diaphragm condition. Since the plate presents a geometric symmetry with respect to its middle surface and by centering the coordinate system so that the middle surface lies in the xy plane, its vibration modes may be classified as symmetric and antisymmetric modes. In the symmetric modes, the in-plane

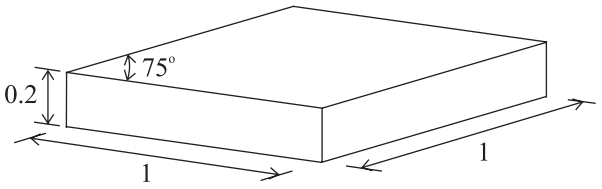

Fig. 2. The skew plate.

displacements are even functions of the z coordinate and the out-of-plane displacement is an odd function of this coordinate. These modes are also called in-plane modes. In the antisymmetric modes, the in-plane displacements are odd functions of the z coordinate and the out-of-plane displacement is an even function of this coordinate. These modes are also called out-of-plane modes. These two types of modes can be determined separately using the h-p version of the finite element method by first centering the coordinate system so that the middle surface of the plate lies in the xy plane and then by discretizing half of the domain above the middle surface into pentahedral p-elements. Appropriate boundary conditions must then be applied on the middle surface. These boundary conditions are $u(x,y,0) = v(x,y,0) = 0$ for the out-of-plane modes and $w(x,y,0) = 0$ for the in-plane modes. Results for the frequency parameters Ω associated with the six lowest out-of-plane and in-plane modes are respectively shown in Tables 2 and 3 along with the values obtained by Liew et al. [1] using the Ritz method. The results were generated from meshes of 2 and 4 elements (Fig. 3) with $p = 2,4,6$, and 8. It is clearly shown that a rapid convergence from above occurs as the number of elements NEL is increased from 2 to 4 and the polynomial order p is increased from 2 to 8 and an excellent agreement with the solution of Liew et al. is obtained using NEL = 4 and $p = 8$ because this solution uses the largest number of degrees of freedom (NDOF = 1310 in in-plane analysis and NDOF = 1133 in out-of-plane analysis).

The second example is a moderately thick cantilevered right isosceles triangular plate with $h = 0.2$ (Fig. 4). The two edges of equal length are free and the other edge is clamped. The clamped edge is restrained in all directions (i.e. the in-plane and out-of-plane displacements are zero). Results for the frequency parameters Ω associated with the 6 lowest out-of-plane and in-plane modes are, respectively, shown in Tables 4 and 5 along with the values obtained by Cheung and Zhou [2] using the Ritz method. The results were generated from meshes of 3 and 6 elements (Fig. 5) with $p = 2,4,6$, and 8. In this case, it is also shown that a rapid convergence from above occurs as the number of elements NEL is increased from 3 to 6 and the polynomial order p is increased from 2 to 8 and an excellent agreement with the solution of

Table 2
Convergence of the six lowest frequency parameters Ω for the out-of-plane modes of the simply supported skew plate

NEL	p	NDOF	Mode no.					
			1	2	3	4	5	6
2	2	28	3.122	15.767	15.767	15.767	16.419	16.457
	4	103	1.726	3.981	5.054	6.109	8.288	9.025
	6	278	1.691	3.576	4.060	5.283	6.708	7.044
	8	601	1.687	3.568	4.038	5.243	6.587	6.833
4	2	47	2.503	5.347	5.605	8.985	10.947	15.767
	4	185	1.699	3.639	4.104	5.458	7.227	7.311
	6	515	1.688	3.568	4.039	5.246	6.605	6.843
	8	1133	1.687	3.567	4.037	5.240	6.583	6.823
Liew et al. [1]			1.687	3.567	4.037	5.240	6.583	6.823

Table 3
Convergence of the six lowest frequency parameters Ω for the in-plane modes of the simply supported skew plate

NEL	p	NDOF	Mode no.					
			1	2	3	4	5	6
2	2	45	4.003	4.638	4.933	6.060	6.578	6.645
	4	144	3.527	3.937	4.565	4.984	5.136	6.026
	6	351	3.504	3.921	4.527	4.874	5.071	6.006
	8	714	3.499	3.920	4.526	4.864	5.064	6.002
4	2	68	3.913	4.219	4.582	5.530	5.792	6.181
	4	242	3.508	3.929	4.528	4.879	5.102	6.014
	6	624	3.499	3.920	4.526	4.864	5.064	6.002
	8	1310	3.497	3.919	4.526	4.862	5.062	6.001
Liew et al. [1]			3.497	3.919	4.526	4.860	5.061	6.001

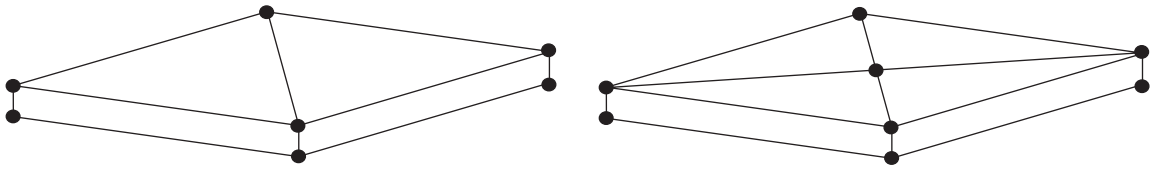

Fig. 3. Meshes for solutions given in Tables 2 and 3.

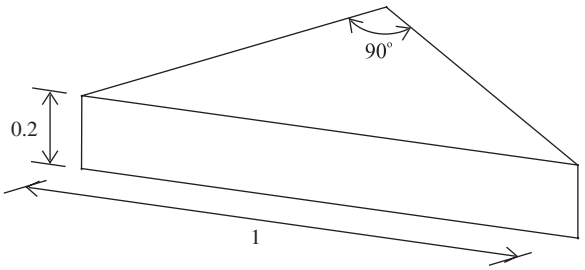

Fig. 4. The right isosceles triangular plate.

Cheung and Zhou is obtained using NEL = 6 and $p = 8$ for all the modes except for the sixth in-plane mode. The value reported by Cheung and Zhou for this mode is an upper-bound to the value calculated by the *h-p* version of the finite element method and is therefore less accurate. Again, the solution which uses NEL = 6 and $p = 8$ is the most accurate because it uses the largest number of degrees of freedom (NDOF = 1673 in out-of-plane analysis and NDOF = 1873 in in-plane analysis).

Table 4
Convergence of the six lowest frequency parameters Ω for the out-of-plane modes of the cantilevered right isosceles triangular plate

NEL	p	NDOF	Mode no.					
			1	2	3	4	5	6
3	2	34	2.219	6.027	7.193	13.672	16.900	18.220
	4	137	2.041	4.604	6.109	9.319	10.359	12.560
	6	384	2.027	4.516	5.987	8.584	9.309	11.270
	8	847	2.025	4.508	5.977	8.529	9.239	11.163
6	2	65	2.120	5.253	6.703	10.175	10.983	12.951
	4	265	2.036	4.545	6.035	8.694	9.406	11.370
	6	753	2.027	4.513	5.985	8.541	9.251	11.175
	8	1673	2.025	4.507	5.977	8.527	9.236	11.160
Cheung and Zhou [2]			2.023	4.505	5.974	8.523	9.234	11.154

Table 5
Convergence of the six lowest frequency parameters Ω for the in-plane modes of the cantilevered right isosceles triangular plate

NEL	p	NDOF	Mode no.					
			1	2	3	4	5	6
3	2	41	4.396	7.358	10.184	13.330	15.373	17.401
	4	163	4.300	6.916	7.932	11.313	12.831	14.057
	6	441	4.297	6.882	7.795	11.090	12.413	13.377
	8	947	4.296	6.880	7.790	11.069	12.357	13.316
6	2	79	4.333	7.011	8.666	11.776	13.680	15.877
	4	317	4.299	6.888	7.810	11.126	12.429	13.460
	6	867	4.297	6.881	7.791	11.072	12.357	13.321
	8	1873	4.296	6.879	7.790	11.068	12.354	13.312
Cheung and Zhou [2]			4.296	6.879	7.790	11.067	12.354	13.406

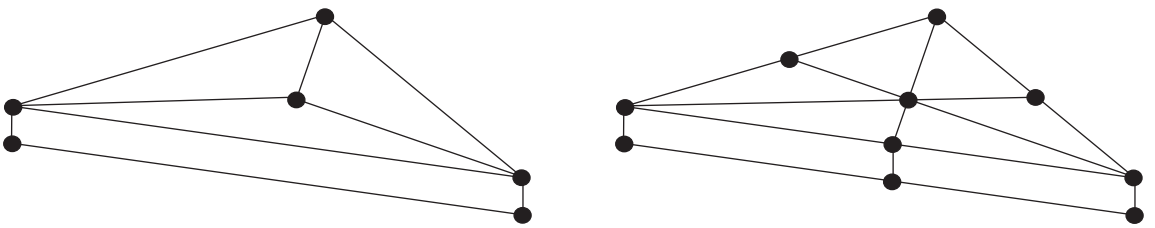

Fig. 5. Meshes for solutions given in Tables 4 and 5.

Table 6
Comparison of the six lowest frequency parameters Ω for the out-of-plane modes of the square plate with a hard edge support condition

h	Method	Mode no.					
		1	2	3	4	5	6
0.01	Present	0.096	0.241	0.385	0.481	0.625	0.866
	Exact Mindlin [6]	0.096	0.241	0.385	0.481	0.625	0.864
	Exact Kirchhoff [7]	0.096	0.241	0.385	0.482	0.626	0.867
0.1	Present	0.931	2.226	3.421	4.172	5.240	6.893
	Exact Mindlin [6]	0.930	2.218	3.402	4.144	5.197	6.821
	Exact Kirchhoff [7]	0.963	2.408	3.853	4.816	6.261	8.669

A third application is to a square plate with $h = 0.01$ (thin) and 0.1 (moderately thick). The plate has a hard edge support condition. Such a support condition means that the supported edge is restrained transversally and tangentially (i.e. the out-of-plane and tangent in-plane displacements are zero). This example is intended to be used as a basis of comparison for two-dimensional plate theories. Results for the frequency parameters Ω associated with the 6 lowest out-of-plane modes are shown in Table 6. The results were generated from a four-element mesh with $p = 8$. The values obtained using Kirchhoff thin plate and Mindlin thick plate theories are also given in Table 6. It can be shown that the agreement between the results of the three methods is excellent in the case of the thin plate because of the fact that thickness effects are less significant in the lower modes of this plate. In the case of the moderately thick plate, significant discrepancies between the three-dimensional values and those obtained using Kirchhoff plate theory appear in all the modes. These discrepancies increase with increasing mode number. This is due to the fact that Kirchhoff plate theory neglects all thickness effects. In the case of the moderately thick plate, the discrepancies between the three-dimensional values and those obtained using Mindlin plate theory are less significant but increase with increasing mode number. This is due to the fact that Mindlin plate theory takes into account transverse shear deformation and rotary inertia but still neglects other thickness effects by assuming, for example, that any line which is originally straight and normal to the middle surface remains straight after deformation.

A further application is to a very thick free hexagonal plate with $h = 0.4$ (Fig. 6). This example is intended to show the applicability of the present method to plates of more complex domains. It appears that no three-dimensional frequencies are reported in the literature for this example. Thus, new three-dimensional frequency values are presented which may be of interest to other investigators. Results for the frequency parameters Ω associated with the 8 lowest out-of-plane and in-plane modes are, respectively, shown in Tables 7 and 8. The results were generated from a six-element mesh (Fig. 7) with $p = 2 - 8$. In this case, a rapid convergence from above is shown to occur as the polynomial order p is increased from 2 to 8 and an accuracy up to three significant digits is reached by using $p = 7$ for the out-of-plane modes and $p = 6$ for the in-plane modes. The frequency parameters in Tables 7 and 8 may serve to validate two-dimensional plate theories and other computational techniques.

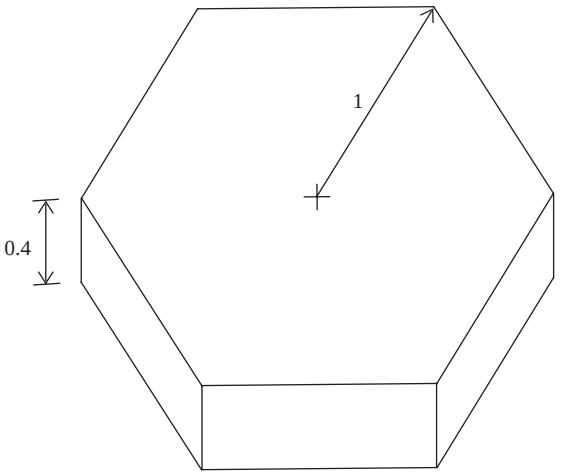

Fig. 6. The hexagonal plate.

Table 7
Convergence of the eight lowest frequency parameters Ω for the out-of-plane modes of the free hexagonal plate

	Mode no.							
p	1	2	3	4	5	6	7	8
2	1.112	1.112	1.808	2.245	2.559	3.516	3.516	4.026
3	1.065	1.065	1.708	1.976	2.446	3.251	3.251	3.469
4	1.054	1.054	1.694	1.925	2.361	3.119	3.119	3.259
5	1.052	1.052	1.693	1.917	2.353	3.103	3.103	3.230
6	1.052	1.052	1.693	1.917	2.352	3.102	3.102	3.226
7	1.052	1.052	1.693	1.916	2.351	3.101	3.101	3.225
8	1.052	1.052	1.693	1.916	2.351	3.101	3.101	3.225

Table 8
Convergence of the eight lowest frequency parameters Ω for the in-plane modes of the free hexagonal plate

	Mode no.							
p	1	2	3	4	5	6	7	8
2	2.607	2.607	3.113	3.113	3.807	4.556	4.761	4.761
3	2.584	2.584	2.945	2.945	3.750	3.860	4.094	4.463
4	2.579	2.579	2.920	2.920	3.748	3.847	4.070	4.363
5	2.578	2.578	2.918	2.918	3.748	3.833	4.060	4.357
6	2.578	2.578	2.918	2.918	3.748	3.831	4.060	4.356
7	2.578	2.578	2.918	2.918	3.748	3.831	4.060	4.356
8	2.578	2.578	2.918	2.918	3.748	3.831	4.060	4.356

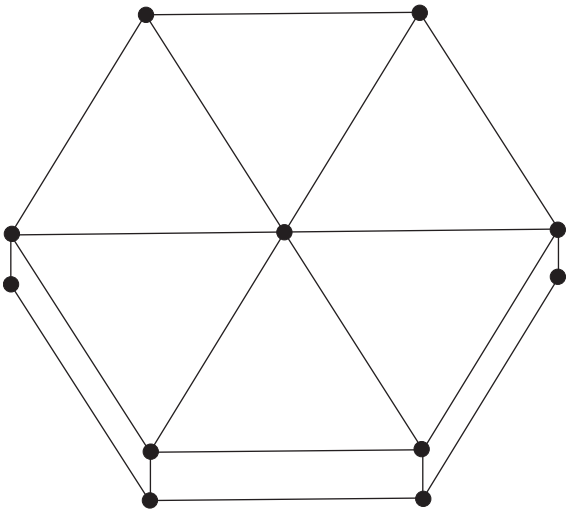

Fig. 7. Mesh for solutions given in Tables 7 and 8.

4. Conclusion

The *h-p* version of the finite element method based on a pentahedral *p*-element has been developed for three-dimensional free vibration of plates. The element's new hierarchical shape functions were expressed in terms of the shifted Legendre orthogonal polynomials. In the *h-p* version of the finite element method, the accuracy of the solution can be improved by simultaneously refining the mesh and increasing the polynomial order. Results of frequency calculations for a skew plate on a soft edge support and a cantilevered isosceles triangular plate using few elements and polynomial orders have illustrated the rapid convergence and high accuracy of the present method. Results were also found for a square plate on a hard edge support and comparisons were made with two-dimensional plate theories. It was found that, in the case of the thin plate, Kirchhoff and Mindlin plate theories produced a similar accuracy in all the modes. In the case of the moderately thick plate, Mindlin plate theory produced a better accuracy than that of Kirchhoff plate theory because it takes into account transverse shear deformation and rotary inertia. The accuracy tended to deteriorate as the mode number increased because Mindlin plate theory still neglects other thickness effects. Furthermore, highly accurate values for a very thick free hexagonal plate were presented for the first time.

Appendix A. Coefficients of $\mathbf{k}_{\alpha,\beta}$ and $\mathbf{m}_{\alpha,\beta}$

$$k_{3\alpha-2,3\beta-2} = \frac{Eh}{4(1+v)(1-2v)} \left\{ \frac{1}{A} \sum_{m=1}^{3} \sum_{n=1}^{3} \left[(1-v) a_m a_n + \frac{(1-2v)}{2} b_m b_n \right] A_{\alpha,\beta}^{m,n} + \frac{8(1-2v)A}{h^2} D_{\alpha,\beta} \right\}, \tag{A.1}$$

$$k_{3\alpha-2,3\beta-1}=\frac{Eh}{4(1+v)(1-2v)}\frac{1}{A}\sum_{m=1}^{3}\sum_{n=1}^{3}\left[va_mb_n+\frac{(1-2v)}{2}b_ma_n\right]A_{\alpha,\beta}^{m,n}, \tag{A.2}$$

$$k_{3\alpha-2,3\beta}=\frac{E}{(1+v)(1-2v)}\sum_{m=1}^{3}a_m\left[vB_{\alpha,\beta}^{m}+\frac{(1-2v)}{2}C_{\alpha,\beta}^{m}\right], \tag{A.3}$$

$$k_{3\alpha-1,3\beta-2}=\frac{Eh}{4(1+v)(1-2v)}\frac{1}{A}\sum_{m=1}^{3}\sum_{n=1}^{3}\left[vb_ma_n+\frac{(1-2v)}{2}a_mb_n\right]A_{\alpha,\beta}^{m,n}, \tag{A.4}$$

$$k_{3\alpha-1,3\beta-1}=\frac{Eh}{4(1+v)(1-2v)}\left\{\frac{1}{A}\sum_{m=1}^{3}\sum_{n=1}^{3}\left[(1-v)b_mb_n+\frac{(1-2v)}{2}a_ma_n\right]A_{\alpha,\beta}^{m,n}+\frac{8(1-2v)A}{h^2}D_{\alpha,\beta}\right\}, \tag{A.5}$$

$$k_{3\alpha-1,3\beta}=\frac{E}{(1+v)(1-2v)}\sum_{m=1}^{3}b_m\left[vB_{\alpha,\beta}^{m}+\frac{(1-2v)}{2}C_{\alpha,\beta}^{m}\right], \tag{A.6}$$

$$k_{3\alpha,3\beta-2}=\frac{E}{(1+v)(1-2v)}\sum_{m=1}^{3}a_m\left[vC_{\alpha,\beta}^{m}+\frac{(1-2v)}{2}B_{\alpha,\beta}^{m}\right], \tag{A.7}$$

$$k_{3\alpha,3\beta-1}=\frac{E}{(1+v)(1-2v)}\sum_{m=1}^{3}b_m\left[vC_{\alpha,\beta}^{m}+\frac{(1-2v)}{2}B_{\alpha,\beta}^{m}\right] \tag{A.8}$$

$$k_{3\alpha,3\beta}=\frac{Eh}{4(1+v)(1-2v)}\left[\frac{1}{A}\sum_{m=1}^{3}\sum_{n=1}^{3}\frac{(1-2v)}{2}(a_ma_n+b_mb_n)A_{\alpha,\beta}^{m,n}+\frac{8(1-v)A}{h^2}D_{\alpha,\beta}\right], \tag{A.9}$$

$$m_{3\alpha-2,3\beta-2}=m_{3\alpha-1,3\beta-1}=m_{3\alpha,3\beta}=\rho hAE_{\alpha,\beta}, \tag{A.10}$$

$$m_{3\alpha-2,3\beta-1}=m_{3\alpha-2,3\beta}=m_{3\alpha-1,3\beta}=m_{3\alpha-1,3\beta-2}=m_{3\alpha,3\beta-2}=m_{3\alpha,3\beta-1}=0. \tag{A.11}$$

References

[1] K.M. Liew, K.C. Hung, M.K. Lim, Vibration characteristics of simply supported thick skew plates in three-dimensional setting, *ASME Journal of Applied Mechanics* 62 (1995) 880–886.

[2] Y.K. Cheung, D. Zhou, Three-dimensional vibration analysis of cantilevered and completely free isosceles triangular plates, *International Journal of Solids and Structures* 39 (2002) 673–687.

[3] D. Zhou, Y.K. Cheung, F.T.K. Au, S.H. Lo, Three-dimensional vibration analysis of thick rectangular plates using Chebyshev polynomial and Ritz method, *International Journal of Solids and Structures* 39 (2002) 6339–6353.

[4] A. Houmat, Free vibration analysis of membranes using the h-p version of the finite element method, *Journal of Sound and Vibration* 282 (2005) 401–410.

[5] B. Szabo, I. Babuska, *Introduction to Finite Element Analysis*, Wiley, New York, 1989.

[6] R.D. Mindlin, A. Schacknow, H. Dereziewicz, Flexural vibrations of rectangular plates, *Journal of Applied Mechanics* 23 (1956) 430–436.

[7] A.W. Leissa, Vibration of plates, NASA-SP-160, 1969.